Journal of Acquired Immune Deficiency Syndromes and Human Retrovirology
18:95–109 © 1998 Lippincott-Raven Publishers, Philadelphia

Role of the Thymus in Pediatric HIV-1 Infection

*Denise E. Kirschner, †Ramit Mehr, and ‡Alan S. Perelson

*Department of Microbiology, University of Michigan Medical School, Ann Arbor, Michigan; †Department of Molecular Biology, Princeton University, Princeton, New Jersey; and ‡Theoretical Division, Los Alamos National Laboratory, Los Alamos, New Mexico, U.S.A.

Summary: Several lines of evidence suggest that HIV-1 is present in the thymus during HIV-1 infection. Precursors to mature $CD4^+$ T lymphocytes develop in the thymus, which suggests that thymic infection may play a role in the $CD4^+$ T-cell decline observed during the course of pediatric HIV-1 infection. We illustrate, through mathematical modeling, the potential effects of thymic infection on the course of pediatric AIDS disease progression. We find that infection in the thymus not only can supplement peripheral infection but can help explain the faster progression in pediatric cases, as well as the early and high viral burden. **Key Words:** Thymus—AIDS—Ordinary differential equations—Immunology—HIV—Pediatric AIDS—Mathematical modeling.

HIV-1–induced immunosuppression is associated with the decline in the level of $CD4^+$ T lymphocytes (1). Within the thymus, thymocytes proliferate and differentiate into $CD4^+$ T cells (2–4). Human thymopoiesis in SCID-hu mice is suppressed by HIV-1 infection, and HIV-1 infection of the thymus may impede regeneration of the peripheral $CD4^+$ T cells (5). Su et al. (6) showed that HIV-1 not only infects and kills $CD4^+$ thymocytes but may also augment apoptosis of uninfected $CD4^+$ thymocytes. Virus isolates that can infect the earlier, less mature thymocytes were shown to cause a more severe disruption of $CD4^+$ T-cell generation in the thymus (6). Thymic epithelial cells can also be infected (7), and this in turn could promote intrathymic spread of HIV-1. Under these conditions, normal nurturing of the developing T cells cannot occur, and patients with AIDS may have smaller than normal thymuses (8,9).

Others have shown (10–13) that vertical transmission of HIV-1 may result in the infection of fetal thymocytes, which can contribute to postnatal HIV-1 associated pathologic conditions. HIV-1–infected children usually progress to AIDS more quickly than adults (14–17). Thymic dysfunction has been a major hypothesis in the study of disease dynamics, and it is thus our aim to explore this phenomenon.

In this work, we explore the consequences of HIV-1 infection of the thymus. We develop mathematical models of interacting immune cells and virus that capture pediatric disease dynamics. One novel finding is that thymic infection can augment peripheral HIV-1 infection; the infected thymus can act as a source of both infectious virus and infected T cells; this may explain the higher viral loads in pediatric patients (18–21). In the following sections, we present a model of thymic infection by HIV-1, addressing pediatric infection, briefly analyze it, and then examine numerical results. We proceed to combine this thymic model with an existing model for the interaction between HIV-1 and peripheral T cells and explore how the infection of the thymocyte population affects the overall dynamics of pediatric infection. We compare our results with available data.

MODEL OF THYMIC INFECTION WITH HIV-1

Model Formulation

Our model includes thymocytes, the precursors to $CD4^+$ T cells, with T_p denoting the number of uninfected

Address correspondence and reprint requests to Denise E. Kirschner, Department of Microbiology and Immunology, University of Michigan Medical School, 6730 Medical Science II, Ann Arbor, MI 48109-0620 U.S.A.; email: kirschne@umich.edu.

Manuscript received December 10, 1997; accepted December 18, 1997.

thymocytes, and T_p^* denoting the number of HIV-infected thymocytes. Because almost all thymocytes express CD4 at some point during their maturation (22,23), we assume that all thymocytes are susceptible to infection. Moreover, because thymocytes are dividing or activated much of the time (3,7), they are likely to become productively infected rather than latently infected. Our model also considers V_T, the total population of HIV-1 particles in the thymus.

The equations describing the time evolution of these populations are as follows:

$$\frac{dT_p}{dt} = s - \delta_{T_p} T_p - e_1 T_p + r_p T_p \left(1 - \frac{T_p + T_p^*}{T_p^{max}}\right) - \beta_p V_T T_p \quad [1]$$

$$\frac{dT_p^*}{dt} = \beta_p V_T T_p - \delta_{T_p^*} T_p^* - e_2 T_p^* \quad [2]$$

$$\frac{dV_T}{dt} = s_V + N_T \delta_{T_p^*} T_p^* - c_V V_T - \beta_p V_T T_p \quad [3]$$

In Equation 1, which describes the change in the uninfected thymocyte population over time, s is a source term representing the rate of homing of bone marrow–derived hemopoietic stem cells to the thymus. Because these cells do not express high levels of CD4, they are less likely to be infected; hence, we assume they supply the thymus at a constant rate. We include the considerable loss of precursor cells due to reasons other than infection by HIV-1 (i.e., thymic selection processes) at per cell rate δ_{T_p} (4,24,25). The next term represents export to the periphery at per cell rate e_1. The extensive proliferation in the thymus is included, at maximum per cell rate r_p. Proliferation is represented in logistic form, to ensure that the maximal allowable number of thymocytes is never exceeded (26). That is, the growth rate (denoted by r_p) is multiplied by a term that approaches zero when the total number of thymocytes approaches the carrying capacity, T_p^{max}. Finally, thymocytes become infected at a rate proportional to the virus population, with a rate constant β_p. Equation 2 models the rate of change of the infected thymocytes; thus, the generation of infected cells, from Equation 1, is the source term in Equation 2. This is followed by a death term of infected thymocytes cells at per cell rate $\delta_{T_p^*}$, and their export with per cell rate e_2.

In Equation 3, thymic virus, V_T, is assumed to be supplied from the periphery at a constant rate s_V. Virus is produced by infected thymocytes, at rate $N_T \delta_{T_p^*}$, where N_T is the average number of viral particles an infected thymocyte produces during its lifetime. We also assume loss of virus from the thymus at per virion rate c_V. This loss could result from clearance (e.g., phagocytosis) within the thymus or to export from the thymus to the periphery. The last term represents the rate of loss of free thymic virus particles due to infection of T_p cells.

Parameter Estimates

We first estimate the input of precursor cells into the thymus. Homing of hemopoietic stem cells in mice occurs at rates of 100 to 200 cells/day (27). Because the human thymus is 3 to 4 orders of magnitude larger than the mouse thymus, we take the source rate in adult humans to be $s = 10^6$ day^{-1}.

The natural death rate for thymocytes is much higher than that of peripheral T cells. Data obtained in mice, and subsequent mathematical analysis, indicate that δ_{T_p} is at least 0.7 day^{-1} (24,25,27). We take the death rate of human uninfected thymocytes to be $\delta_{T_p} = 0.7$ day^{-1}. The death rate of infected thymocytes should be at least as high. Published work (28) gives a minimum estimate for the death rate of infected peripheral T cells to be 0.5 day^{-1}, and the death rate for thymocytes due to infection is likely to be higher, inasmuch as they are more sensitive to induced cell death (6). Taking all these factors into account, we choose $\delta_{T_p^*} = 1.5$ day^{-1}.

The number of thymocytes in the human thymus has been estimated, maximally, based on mouse data, to be on the order of 5×10^{10} (29); hence, we use this value for T_p^{max}, although it may be smaller. We choose our initial condition for the number of thymocytes in an uninfected individual to be less than the maximal value, namely $T_p(0) = 2.5 \times 10^{10}$. The growth rate of thymocytes is on the order of 1.0/day^{-1} to 1.5/day^{-1} (24); here, we choose $r_p = 1.5$ day^{-1}.

The thymic export rates of uninfected and infected CD4$^+$ T cells, e_1 and e_2, respectively, are estimated based on numbers of new thymic emigrants. Shortman et al. (27) showed in mice that at most 0.5% to 2% of any cohort of thymocytes leave the thymus and enter the CD4$^+$ or CD8$^+$ mature T-cell population in the periphery. Our choice of $e_1 = 0.04$ day^{-1} for the per-cell rate of thymic export of CD4$^+$ T cells is based on the fact that it gives a reasonable uninfected steady state thymus size.

No available data consider the rate at which infected thymocytes are exported to the periphery, if at all. We assume that it is either equal to or smaller than the export rate of uninfected thymocytes, because infected thymocytes may not be as responsive to maturation signals as uninfected thymocytes. In our simulations, we used $e_2 = 0.02$ day$^{-1} < e_1$; however, choosing $e_2 = 0$ has little effect on the overall dynamics.

From in vitro data, it has been estimated that approximately 1% to 2% of thymocytes become infected per day (23). However, the in vivo extracellular concentration of virus may be lower than that of in vitro infection, and evidence suggests that cells in vivo produce fewer virus particles before they die than cells in vitro (30), possibly as a result of elimination of infected cells by immune response mechanisms. In any case, the available data do not enable us to determine independently the rate constant for infection (β_p) and the number of virus particles produced per infected thymocyte (N_T). In our simulations, the choices of β_p are on the order of 10^{-10} day^{-1}, and N_T is on the order of 100, based on data from Haase et al. (30). This resulted in realistic disease dynamics (discussed later).

No data are available on the rate of transport of free virus between the blood and the thymus. If no virus enters the thymus, that is, $s_V = 0$, then, with our default parameters, infection in the thymus is not sustained and the system (1–3) moves toward the uninfected steady state. In our simulations, we used values of s_V up to the order of 10^9 day^{-1}, that is, up to 10% of the estimated daily production of HIV-1 (31). Finally, the sum of viral clearance within the thymus and viral export from the thymus is estimated through simulations to be on the order of $c_V = 100$ day^{-1}. These parameter definitions and default values as described previously are given in Table 1. The effects of varying the parameters for which data are scarce were studied through simulations and are presented later in this paper. A brief mathematical analysis of the model is presented in the Appendix.

Thymus Model Simulations

We examine numerical solutions of Equations 1, 2, and 3. Parameter values are listed in Table 1 unless otherwise specified. In Figure 1, we show simulations with $N_T = 100$ and $\beta_p = 7.5 \times 10^{-11}$ day^{-1}, and two extreme cases of viral influx into the thymus: $s_V = 10^9$ day^{-1} (Fig. 1*A*) and $s_V = 10$ day^{-1} (Fig. 1*B*). Figure 1 shows that the value of $s_V > 0$ has a negligible effect on the final, infected steady state, and only a small effect on the time to reach this steady state. In the model, infection in the adult thymus happens quickly, that is, within 2 to 4 weeks, which agrees with data reported by Autran et al. (32). The total number of precursor cells drops to half of the initial value within a month after virus is introduced into the thymic environment and stabilizes at this level. This is consistent with findings on autopsies of HIV-1–seropositive and AIDS patients, indicating that the depletion of the thymus is at most on the order of twofold (33). In the simulation, the viral load in the thymus becomes very large during this first month, increasing from zero to the order of 10^9. This large viral load is also consistent with recent measurements of viral load in lymphoid tissue as well as modeling approximations (30,34–36).

The parameters N_T and β_p must lie in a certain parameter region for thymic infection to be established (see Appendix for mathematical discussion). Figure 2*A* shows the dependence of the steady state on the value of N_T. For a fixed value of $\beta_p = 7.5 \times 10^{-11}$ day^{-1}, as the value of the viral production per cell, N_T, increases up to 200, the infection becomes more severe and is also established

TABLE 1. *Variables and parameters for the thymus model, Equations 1 through 3*

Dependent Variables		Initial Values
T_p	= Uninfected precursors to CD4$^+$ T cell population	2.5×10^{10}
T_p^*	= Infected precursors to CD4$^+$ T cell population	0.0
V_T	= HIV population in thymus compartment	0.0
Parameters and Constants		Values
δ_{T_p}	= death rate of precursor cell population	0.7 day^{-1}
$\delta_{T_p^*}$	= death rate of infected precursor population	1.5 day^{-1}
r_p	= rate of growth for the precursor population	1.5 day^{-1}
N_T	= number of free virus produced per T_p^*	100
T_p^{max}	= maximum precursor population level	5×10^{10}
s	= source term for hemopoietic cells	1×10^6 day^{-1}
e_1	= rate precursor cells differentiate into CD4$^+$ T cells	0.04 day^{-1}
e_2	= rate infected precursor cells differentiate into T^*	0.02 day^{-1}
β_p	= rate precursor cells become infected by free virus	0.75×10^{-10} day^{-}
c_V	= rate free virus cleared from thymus[a]	100 day^{-1}
s_V	= rate virus flows into thymus[a]	up to 10^9 day^{-1}

$T_p^{max} = 2.5 \times 10^{10} W(t) R(t)$: age-dependent precursor maximum
$R(t) = 0.01 \times (0.2825 e^{-0.001481t} + 0.1358)$: ratio of thymus weight to body weight
$W(t) = (3.0 + 0.4\sqrt{t})$: body weight in kg at age t

[a] Parameter is used in the thymus-only model but not in the full, combined model.

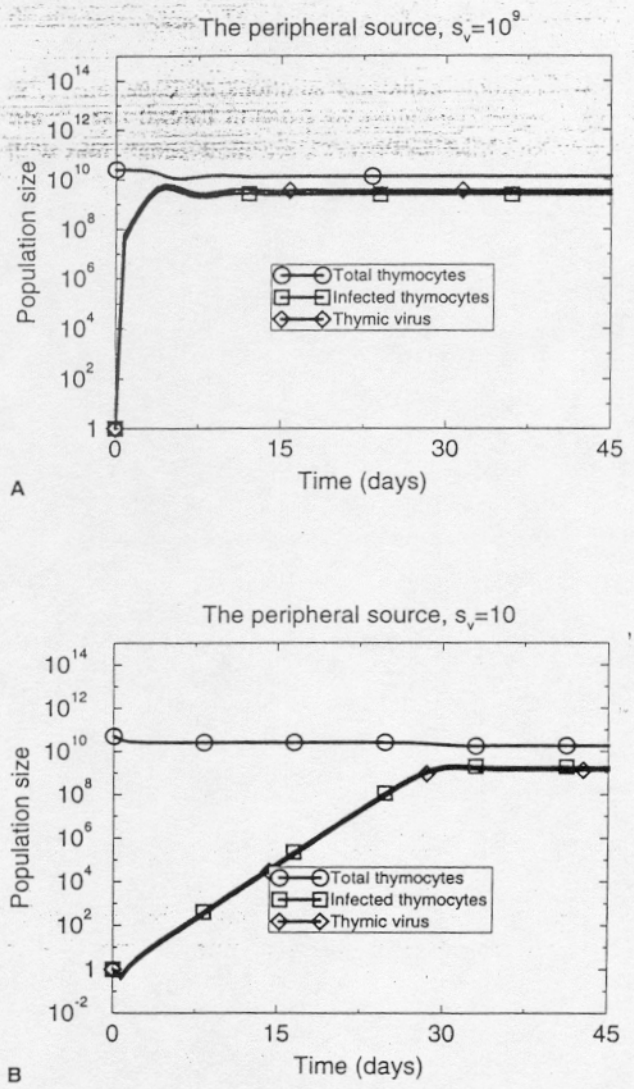

FIG. 1. The thymic infection model. Numerical solution of the thymus model, Equations 1 through 3, with parameter values as given in Table 1. To examine different viral flow rates from the periphery into the thymus, we compare (**A**) $s_V = 10^9$, (**B**) $s_V = 10$. In either case the steady state value for the thymocyte populations is the same after 30 days.

faster based on high viral loads and T-cell counts (data not shown). Conversely, with a low value of N_T on the order of 10, the infection level is so low that the number of thymocytes is hardly decreased.

Figure 2*B* presents the case in which the value of N_T is fixed, $N_T = 100$, and β_p is varied from 10^{-11} day^{-1} to 9×10^{-11} day^{-1}. As β_p is reduced, the approach to the steady state slows down (not shown) and the final level of infection decreases. For sufficiently low values of β_p, the infection does not become established in the thymus.

The dependence of the steady state values on other parameters is summarized in Table 2. Obviously, increasing the default death rate or the export rates of thymocytes results in lower steady state levels of thymic infection, as does a reduction in the thymocyte population growth rate. One parameter for which we have no data is c_V, the rate of viral clearance within the thymus and/or export from the thymus. It is clear, however, that with higher values of c_V, the infection will be slower, and vice versa. The issue of viral traffic between the thymus and periphery is explored in more detail later in this paper.

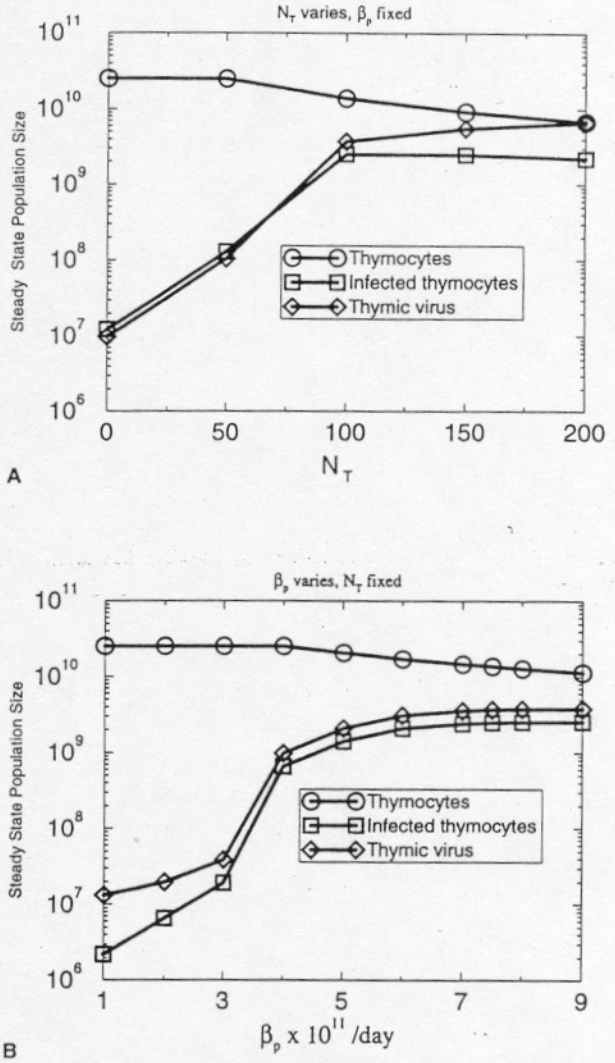

FIG. 2. This figure explores the role of the parameters N_T and β_p on infection. (**A**) For a fixed value of $\beta_p = 7.5 \times 10^{-11}$ day^{-1}, as the value of the viral production per cell, N_T, increases from 10 to 200 the infection becomes more severe. Conversely, with a low value of N_T, of the order of 10, the infection level is so low that the number of thymocytes is unaffected. (**B**) For a fixed value of $N_T = 100$, as the value of the viral infection rate, β_p, increases from 9×10^{-11} to 10^{-11} day^{-1} the steady state level of infection decreases. For low enough values of β_p, the infection does not establish in the thymus.

TABLE 2. *Parameter sensitivity of the thymus model. Effect on steady state of change in default value[a] when parameter is: increased (doubled) and decreased (halved)*

Parameter	Increase	Decrease
s	NC	NC
δ_{T_p}	SS (L)	SS (H)
e_1	LSS	NC
e_2	LSS	NC
r_p	SS (H)	LSS
T_p^{max}	SS (H)	SS (L)
β_p	LSS	NI
$\delta_{T_p^*}$	SS (L)	SS (H)
s_V	NC	NC
N_T	LSS	HSS
c_V	NI	LSS

NC, No substantial change in steady state (SS) value; LSS, a lower SS is reached (all variables); HSS, a higher SS is reached (all variables); SS (L), T_p remains in SS, but V_T, T_p^*, are at a lower SS value; SS (H), T_p remains in SS, but V_T, T_p^*, are at a higher SS value; NI, no infection in thymus by day 60.

[a] Default values are shown in Table 1.

These different steady state outcomes resemble the experimentally observed virus strain–dependent difference in the levels of infection (8). The model thus suggests that a low virus production is not powerful enough to cause substantial infection of the thymus and depletion of thymocytes. The infected thymus, however, could still export virus and infected T cells to the periphery. Because of the immune elimination of HIV-infected cells, the average viral production, N_T, is probably lower in the thymus than that observed in vitro or in hu-SCID implants. Additionally, we expect viral production in thymocytes to be lower than that in peripheral T cells, because thymocytes are more easily triggered into programmed cell death (i.e., apoptosis), especially as a result of cross-linking of their CD4 surface molecules (37,38). Thus, simulations with higher values of N_T may represent the situation in vitro and in the hu-SCID model, whereas lower values may represent the situation in the infected human thymus (Fig. 2*A*).

Pediatric Infection With HIV-1 in the Thymus

As more information becomes available about HIV and AIDS, it is clear that pediatric infection is not only an increasing problem but also seems to have a different pathway to disease than adult infection (14–17). The main transmission route is vertical, from mother to child during pregnancy or at birth, although cases exist in which children become seropositive after birth. Because the child's immune system, including the thymus, is in the early stages of development, differences may be expected between adult and pediatric infection. HIV-1 infection in pediatric patients usually proceeds much faster than in adults. For example, in prenatally infected patients, $CD4^+$ T-cell numbers in the peripheral blood decrease from about 2000/mm^3 at birth to <500/mm^3 within a year, compared with a decrease from about 3000/mm^3 at birth to about 1800/mm^3 at 2 years in healthy infants (14–17,39,40).

To explore the dynamics of pediatric infection, we must adjust for the pediatric physical proportions, and for the fact that the pediatric patient is undergoing tremendous growth. Using data (41–44), we estimate the change in size of the pediatric thymus with respect to age as follows. Total body weight as a function of age is found in standard growth charts from birth (45). A reasonable fit to these data is obtained using the function $W(t) = (3.0 + 0.4\sqrt{t})$, where $W(t)$ is body weight in kilograms and t is age in days (Fig. 3*B*). Data from Cardarelli (42) on the thymus weight as a fraction of body weight can be fit with the function $R(t) = 0.002825e^{-0.001481t} + 0.001358$ (Fig. 3*A*) (46). Converting units, $10^3 \cdot W(t)R(t)$ is the thymus weight in grams. We assume that the number of thymocytes scales with thymus weight until puberty. We therefore replace the constant, maximum thymocyte population size, T_p^{max}, in Equation 1 by the function $T_p^{max}(t) = 2.5 \times 10^{12} W(t)R(t)$ (Fig. 3*C*); the adult thymus weighs about 20 grams and contains about 5×10^{10} cells at its peak size (i.e., contains 2.5×10^9 cells/g).

A numerical simulation of the thymus model with the time varying $T_p^{max}(t)$, assuming infection at birth, gives the results shown in Figure 4. Infection within the growing pediatric thymus progresses more slowly than the adult thymus, probably because infection has to "catch up" with the fast production of new thymocytes. However, because the thymus plays a more significant role in the production of T cells for the pediatric immune system, thymic infection may still exacerbate the course of HIV-1 infection, as shown later in this paper.

ROLE OF THYMUS IN OVERALL IMMUNE DYNAMICS

Plasma-Thymus Combined Model

Perelson (47) presented a simple model for the interactions of HIV-1 with T cells. These results were later extended analytically and some of the model's behavior is explored by simulation by Perelson et al. (48). The model exhibited many of the characteristics of AIDS seen clinically: the long latency period and the depletion of $CD4^+$ T cells. The source for $CD4^+$ T cells in this model was either a constant, sT, or a phenomenologically chosen function of the viral load, $s_T/\theta+V$,

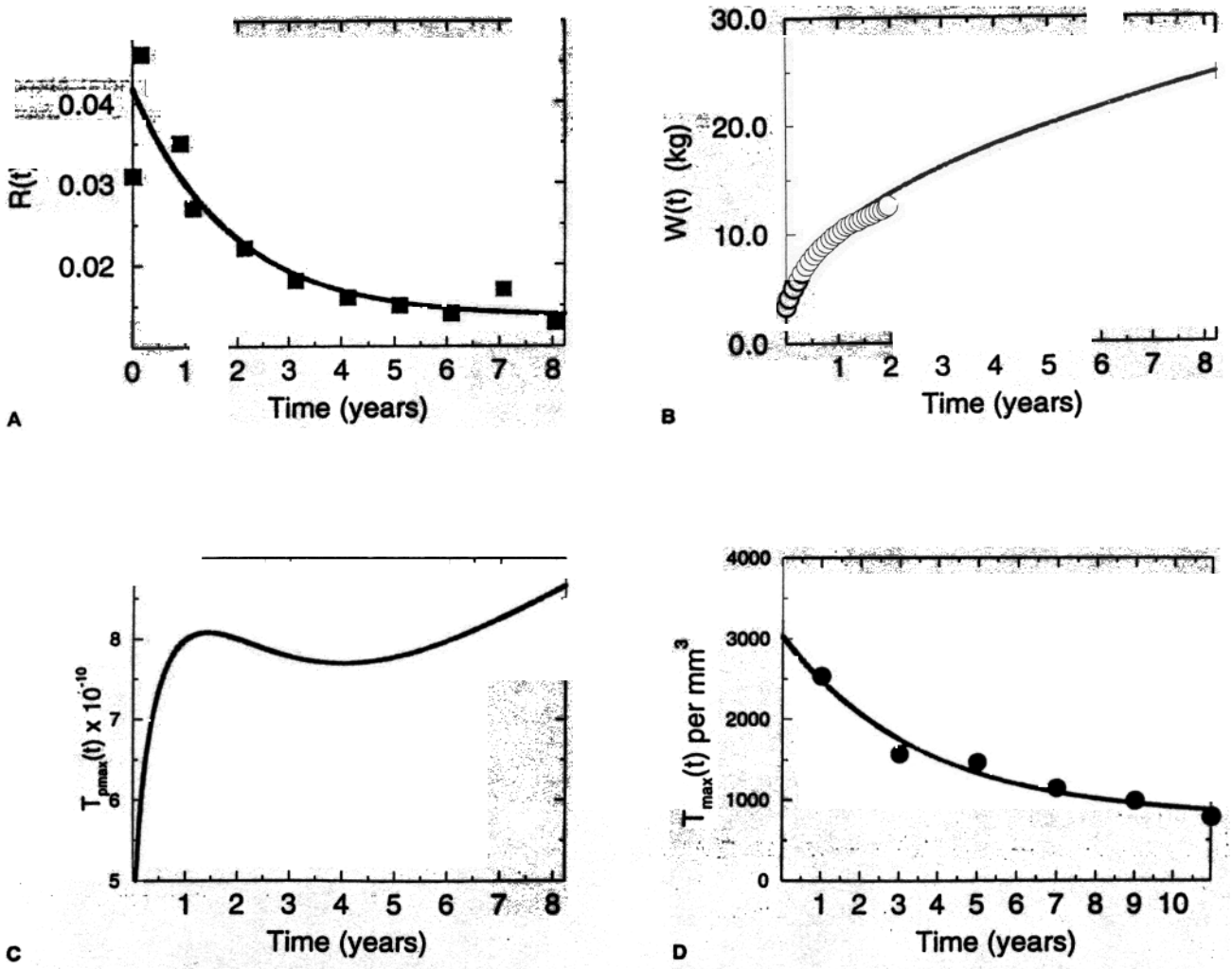

FIG. 3. These are the functions used to determine the course of growth of the pediatric thymus: (A) $R(t)$, (B) $W(t)$, (C) $T_p^{max}(t)$, and (D) $T_{max}(t)$. The functions $R(t) = 0.002825e^{-0.0014611t} + 0.001358$, $T_{max}(t) = 771 + 2258e^{-t/1300}$ and $W(t) = 3 + 0.4\sqrt{t}$ were estimated from data, which are also shown. The function $T_p^{max}(t) = 2.5 \times 10^{12} W(t)R(t)$ is explained in the section on Pediatric Infection with HIV-1 in the Thymus.

where θ is constant, which decreased as the viral load increased. This decreasing source is meant to account for thymic infection. The model required that T cells first become latently infected and then on activation become productively infected. New data on the rapid dynamics of HIV infection (29,32,49) suggest that some of the cells bypass the latently infection stage. Here, following the work of McLean et al. and Phillips (50,51), we incorporate this feature into the original model (47), and combine the modified version of this model with our model for thymic infection. The resulting model is novel in that it considers the transport of cells and virus between the blood and a lymphoid compartment and illustrates how concentrations need to be scaled when tissue and blood are studied.

Let T denote the peripheral blood concentration of uninfected CD4$^+$ T cells, and let T^* and L denote the concentrations of productively infected and latently infected CD4$^+$ T cells, respectively. The blood concentration of free virus particles is denoted by V. A summary of the definitions and numerical information for the parameters and functions appearing in the new equations can be found in Table 3, as well as a discussion in the following section. The new model of thymus-plasma dynamics is given by:

$$\frac{dT_p}{dt} = s - \delta_{T_p} T_p - e_1 T_p + r_p T_p \left(1 - \frac{T_p + T_p^*}{T_p^{max}}\right) - \beta_p V_T T_p \quad [4]$$

$$\frac{dT_p^*}{dt} = \beta_p V_T T_p - \delta_{T_p^*} T_p^* - e_2 T_p^* \quad [5]$$

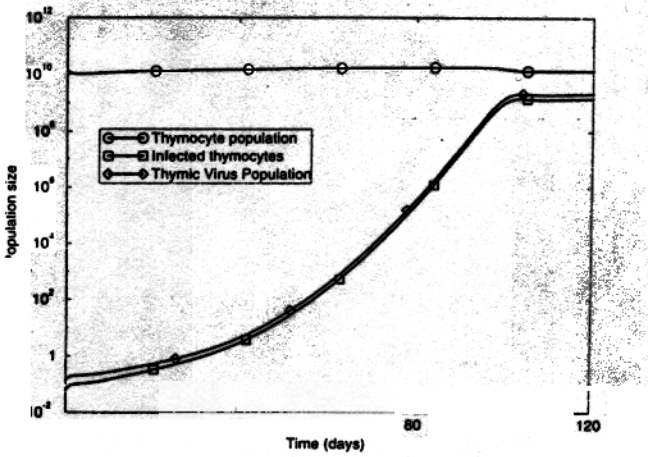

FIG. 4. Pediatric thymic infection. Numerical solution of the thymus model (1)–(3) with the constants T_{max} and T_p^{max} replaced by the functional forms shown in Figure 3. Parameters are as in Table 1, and the initial values are $T_p(0) = 2 \times 10^{10}$, $T^*_p = 0$, $V_T(0) = 0$. In the simulations described here, we assumed that the mode of transmission is vertical, so that HIV is present in the blood at birth. The values for total thymocytes, infected thymocytes and thymic virus are given.

$$\frac{dT}{dt} = be_1T_p - \delta_T T + rT\left(1 - \frac{T+L+T^*}{T_{max}}\right) - \beta VT \quad [6]$$

$$\frac{dL}{dt} = f\beta VT - \delta_L L - aL \quad [7]$$

$$\frac{dT^*}{dt} = be_2T_p^* + aL - \delta T^* + (1-f)\beta TV \quad [8]$$

$$\frac{dV}{dt} = N(t)\delta T^* - cV - \frac{q}{F_{EC}}\left(V - \frac{V_T}{F_T}\right) - \beta VT$$

$$\frac{dV_T}{dt} \quad q\left(V \quad \frac{V_T}{F_T}\right) + N_T(t)\delta_{T_p^*}T_p^* \quad \delta_V V_T - \beta_p V_T T_p \quad 10]$$

where

$$N(t) = N_T(t) = N_0\left(1 + \frac{2.5t^2}{(1.5 \times 10^6 + t^2)}\right) \quad [11]$$

Equations 4 and 5 are identical to Equations 1 and 2. Equation 10 is similar to Equation 3, except the viral transport between the thymus and the peripheral blood is made more explicit, that is, s_V has been replaced by the term $q(V - V_T/F_T)$. These thymic equations, (4,5,10), are written in terms of the total number of cells and virions in the thymus, whereas the equations for T, L, T^* and V in the periphery, Equations 6 through 9, are in units of cells per cubic millimeter of blood; in our graphic output, we present V in the standard units of virions per milliliter. Thus, to properly scale the exchanges of cells between compartments, we divide the number of thymic cells exported to the blood by the total blood volume, B, and multiply by 0.02, because only about 2% of the newly produced T cells remain in the blood. Hence, in Equations 6 and 8, the thymic export terms, e_1T_P and $e_2T_p^*$ are multiplied by $b = 0.02/B$.

An analogous scaling is required in Equations 9 and 10 for the virus transport terms. For simplicity, we regard the thymus as a well-mixed container of cells and fluids (blood and extracellular fluid). We assume fluid flows through the thymus at rate q mm^3/day carrying virus with it. Thus, if the virus concentration is V virions/mm^3, qV virions enter the thymus each day. Assuming free virions are distributed throughout the extracellular fluid of the body, this causes a decrease in the extrathymic virion concentration of qV/F_{EC}, where F_{EC} is the volume of extracellular fluid in the body. Within the thymus the number of free virions is V_T, hence the virion concentration is V_T/F_T, where F_T is the volume of thymic extracellular fluid. Fluid flow through the thymus at rate q thus carries qV_T/F_T virions out of the thymus per day. These virions get diluted in the extracellular fluid of the body, and hence increase in the blood virus concentration at rate $qV_T/(F_TF_{EC})$.

The thymus is only roughly represented by a well-mixed reservoir of virus particles, and hence the parameters q and F_T should be interpreted as "effective" parameters that describe the transport process. Thus, q summarizes flow of both blood and extracellular fluid and F_T is a scaling parameter that determines the concentration of virions carried out of the thymus. If we let $k_V = q/F_{EC}$, then k_V is the rate at which virions are transported into the thymus. Because virions may be trapped in the tissue, the effective concentration may be less than the total number of virions divided by the true extrathymic fluid volume. However, in the absence of experimental measurements, we use the previously described estimate for F_T.

In Equation 6, r represents the population growth rate of T cells, which is again modeled as a logistic growth. T cells have a finite life span and die with rate δ_T per cell (Equation 6). In Equation 7, latently infected T cells die with a rate per cell δ_L, which may be larger than δ_T. If these cells express some viral proteins, immune mediated destruction can augment their natural death rate.

The other terms in Equations 6 and 7 deal with the effects of HIV. The term βVT models the rate that free virus, V, infects CD4$^+$ T cells. After a T cell has been infected, it becomes a latently infected cell, L, with probability f, or a productively infected T cell, T^*, with probability $(1 - f)$. Equation 8 models the productively in-

TABLE 3. *Variables and parameters for the combined model, Equations 4 through 10*

		Dependent variables	Initial values
T	=	Uninfected CD4$^+$ T cell population[a]	1173 mm^{-3}
L	=	Latently infected CD4$^+$ T cell population	0.0
T^*	=	Productively infected CD4$^+$ T cell population	0.0
V	=	HIV plasma population	1.0 × 10^3 mm^{-3}
		Parameters and Constants	Values
δ_T	=	death rate of uninfected CD4$^+$ T cells	0.01 day^{-1}
δ_L	=	death rate of latently infected CD4$^+$ T cells	0.01 day^{-1}
δ	=	death rate of productively infected CD4$^+$ T cells	0.5 day^{-1}
c	=	virus clearance rate in plasma	6 day^{-1}
δ_V	=	virus clearance rate in thymus	4 day^{-1}
β	=	rate CD4$^+$ T cells become infected by free virus	9.5 × 10^{-7} mm^3 day^{-1}
a	=	rate T^* cells convert to productively infected cells	3 × 10^{-5} day^{-1}
r	=	rate of growth for the CD4$^+$ T cell population	0.03 day^{-1}
N_0	=	number of free virus produced by T^* cells	0, 100, 150, 500
f	=	fraction of infections that lead to latently infected cells	0.05
q	=	rate fluid flows into and out of thymus	.1 × F_{EC} mm^3 day^{-1}
		Adult Values	
T_{max}	=	maximum CD4$^+$ T cell population level	1.5 × 10^3 mm^{-3}
B	=	blood volume	5 × 10^6 mm^3
F_{EC}	=	vol. of total-body extracellular fluid	15 × 10^6 mm^3
F_T	=	vol. of thymic extracellular fluid	4300 mm^3
b	=	$0.02 \times \frac{1}{B}$, because only 2% of thymocytes remain in blood	mm^{-3}
$T_{max}(t)$	=	$771 + 2258e^{-t/1300}$	
$B(t)$	=	$7 \times 10^4\ W(t)$	
$F_{EC}(t)$	=	$\frac{15 \times 10^6\ \text{mm}^3}{70\text{kg}} \cdot W(t)$	
$F_T(t)$	=	$\frac{4300\ \text{mm}^3}{.02\text{kg}} \cdot W(t) \cdot R(t)$	

[a] Uninfected steady-state value.

fected CD4$^+$ T population. At rate aL, latently infected cells become productively infected. Productively infected cells produce virus and die at per cell rate δ.

Equation 9 models the free virus population. We assume that when a productively infected CD4$^+$ T cell becomes stimulated through exposure to antigen, replication of the virus is initiated, and an average of N virus particles are produced before the host cell dies. Because of viral evolution in an infected host, we allow N to increase over the course of infection to account for increased efficiency of viral replication over the long-term infection (see Eq. 11; discussed later). The next term, $-cV$, accounts for viral loss due to decay of virions or their clearance. A separate term is given for the loss of virus as a result of transport into the thymus. Note that there will be a net transport of virus into the thymus when its blood concentration is higher than its thymic concentration. The last term accounts for the loss of free virus particles that infect T cells.

Pediatric Parameters for the Thymus-Plasma Model

To specify the model shown in Equations 4 through 10 as a pediatric model, we must ensure all the parameters that may be age-dependent are modeled to represent pediatric infection accurately. Therefore, we use T_p^{max}, the carrying capacity for the thymocyte population, as defined in the discussion of Pediatric Infection With HIV-1 in the Thymus (Fig. 3*C*). For this plasma-thymus model of pediatric HIV-1 infection, we must also take into account other age-dependent functions.

First, the T-cell numbers change with respect to age. We choose $T_{max}(t) = 771 + 2258e^{-t/1300}$ (Fig. 3*D*). This function is obtained by fitting data from Bofill et al. (39) and from McKinney and Wilfert (46) on changes in the average T-cell count with age. In our model, the steady state T-cell count is lower than T_{max}; however, the variability between humans is sufficiently wide that in using this data we find that both $T_{max}(t)$ and the steady state T-cell count lie within the observed range.

Second, the volume of extracellular fluid in the body, F_{EC}, must also be age dependent. For the average adult weighing 70 kg, we assume $F_{EC} = 15 \times 10^6 \text{mm}^3$; however, for the age-dependent extracellular fluid, we use the age-dependent formula in Equation 12, recalling from the section on Pediatric Infection With HIV-1 in the Thymus that we estimated the age-dependent body weight, $W(t)$ (Fig. 3*B*):

$$F_{EC}(t) = \frac{15 \times 10^6 \text{mm}^3}{70\text{kg}} \; W(t) \qquad [12]$$

Third, based on the ratio of thymus weight (20 g) (52) to total body weight (70 kg), we deduce that in an average adult, the thymic extracellular fluid volume is F_T = 4300 mm^3; however, for the age-dependent thymic fluid, we use the formula in Equation 13, recalling from the section on Pediatric Infection With HIV-1 in the Thymus that we estimated both $R(t)$ and $W(t)$ (Fig. 3*A*, *B*):

$$F_T(t) = \frac{4300\text{mm}^3}{.02\text{kg}} \; W(t) \cdot R(t) \qquad [13]$$

where $R(t)$ is the thymus to body weight ratio.

Fourth, we can estimate the change in blood volume with respect to age, assuming that total blood volume scales with total body weight. For the average 70-kg person the blood volume is 5 L, or 7 × 10^4 mm^3/kg. Thus, we assume the blood volume, $B(t)$, expressed in cubic millimeters, is $B(t)$ = 7 × 10^4 $W(t)$, where $W(t)$ is the age-dependent body weight described in the section on Pediatric Infection with HIV-1 in the Thymus (Fig. 3*B*).

Fifth, we need to estimate the infection rate constant in the pediatric thymus as well as in the plasma. The value we used in the adult thymus model, Equations 1 through 3, is β_p = 7.5 × 10^{-11} per day. In Figure 2*B*, we presented results for varying values of β_p over the range 1 × 10^{-11}/day^{-1} – 9 × 10^{-11}/day^{-1}. This corresponds with a range for the infection rate $\beta_p T_p$, of approximately 0.1 – 1.0 d^{-1}. For plasma infection, we must also estimate a value for β, representing viral infection of plasma T cells. A value that gave realistic output for these simulations is β = 9.5 × 10^{-7} mm^3/day. This implies that βT (range, 10^{-4}/day^{-1} to 10^{-3}/day^{-1}) is as much as 1000-fold higher than $\beta_p T_p$. This large difference can be justified by the difference in T-cell density between the thymus and the blood. Assuming that the density of the human thymus is comparable with that of the murine thymus, that is, 10^7 thymocytes in a volume of the order of 10 mm^3 (27), we estimate the thymic density by 10^6 cells/mm^3, which is 1000-fold larger than the density of T cells in the blood. Hence, a 1000-fold smaller thymic infection rate is sufficient to maintain a similar level of infection in both compartments.

Finally, other parameters in the model shown in Equations 6 through 9 were estimated previously in separate studies by Perelson et al. (48). We summarize all parameter values in Tables 1 and 3. We now present the combined model results.

Results of Pediatric Thymus-Plasma Model

A representative numerical simulation of pediatric infection, in which N_0 = 350 (Eq. 11), is shown in Figure 5*A*, *B*. Pediatric-specific parameters are estimated in the preceding section and all others are presented in Table 3. The other parameter values were chosen based on previous modeling efforts (47,48), and recent experimental studies (28,31).

The course of infection is more rapid than in adults. In the thymus-only model, the thymic infection took 4 months to establish (Fig. 4); the effects on the thymus–plasma dynamics are that thymic infection is increased, taking place in <2 months. This may be accounted for by the nonmechanistic way in which we modeled plasma-viral input as constant in the thymic-only model (Equa-

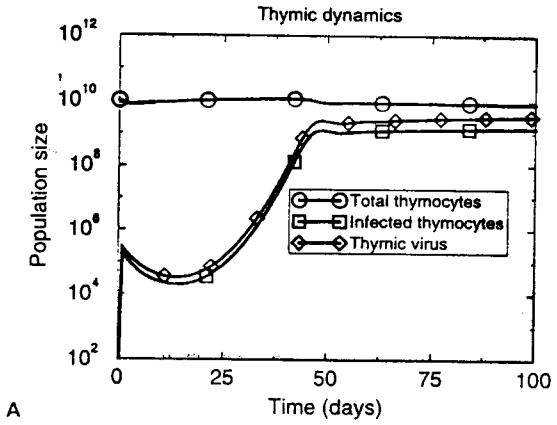

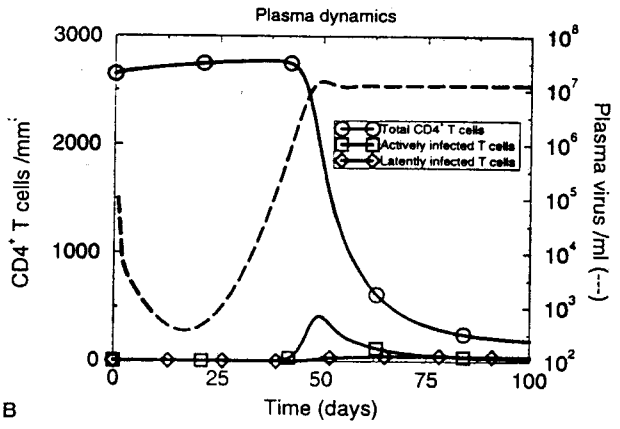

FIG. 5. The pediatric combined thymus-plasma model: a numerical solution of the pediatric combined model using the functions presented in Figure 3. Parameter values are as given in Tables 1 and 3. (**A**) The dynamics in the thymus compartment. (**B**) The dynamics in the plasma.

tion 3) as compared with the more mechanistic combined model (Equation 10). For lower values of N_0 we can achieve slower disease progressions. These variable results are in agreement with the range of different clinical pictures seen in pediatric patients (40). The dynamics of this model yield a low plasma CD4$^+$ T-cell count, together with an early and high viral load. These viral load phenomena are characteristic of pediatric patients (18–21,40). The simulations also exhibit an early and sudden decrease in thymocyte numbers by approximately twofold, and a subsequent decrease in total peripheral CD4$^+$ T cells over a 100-day disease duration. Only a small fraction of CD4$^+$ T cells is latently or productively infected at any given time, as has been seen experimentally (53).

Kourtis et al. (14) explored the role of the thymus in HIV-infected pediatric cases. They examined HIV-1–infected infants whose T-cell and B-cell populations had characteristics similar to that seen in infants with congenital thymus deficiency (DiGeorge syndrome), that is, low CD4$^+$ and CD8$^+$ T-cell counts and low CD5$^+$ B-cell counts. They found that HIV-1–infected infants with this phenotype, which is characteristic of thymic deficiency, progressed to AIDS more rapidly than HIV-1–infected infants without the phenotype. The data are shown in Figure 6 and compared with the results of our model. Our model captures the behavior of the clinical data. The difference between the various pediatric cases may lie in the time since infection. The earlier infection occurs during pregnancy, the more severe the thymic damage will be at birth, and hence the faster the progression to AIDS. We capture this in our model by assuming the initial viral burst size, N_0, is large (see plot in Fig. 6 with $N_0 = 500$). In contrast, infection, and the resulting thymus infection, which occurs later in fetal development or neonatally, may correspond to a less severe postnatal infection. This is captured by assuming a lower viral burst size at birth, that is, $N_0 = 100$. Further, the study by Kourtis et al. (14) is consistent with the notion that the disease course in infants can be severely augmented by infection in the thymus. Note that varying the infection rate β can also yield similar results as with varying N_0; hence, βN_0 dictates the strength of injection.

The transport of viral particles between the thymus and periphery is also explored. Our basic assumption is that the rate of transport of viral particles between the blood and the thymic extracellular fluid depends on the rate of fluid flow, q, into the thymus as well as the virion concentration in the extracellular fluid. The rate of flow is not known, and hence is one of the parameters we studied in our simulations. Our results reveal an interesting phenomenon. As long as q is large enough ($\geq .01 \times F_{EC}$/day) thymic infection is quickly established and the thymus becomes a source of virus. Under these circumstances, thymic infection may then augment peripheral infection. In this parameter regime, the higher q, the faster the rate at which virus is transported out of the thymus and hence the lower the thymic virus. This leads to a slower infection in the thymus, so that by the end of our simulation time (2 years for pediatric infection at birth) the degree of infection in the thymus is lower (Fig. 7A). However, because of the increased transport of virus into the periphery as q increases, peripheral viral loads increase and peripheral T-cell counts decrease (Fig. 7). Data from Shearer et al. (40) show viral load levels versus time for a cohort of 106 children. Their viral loads show an early rise and tendency toward an equilibrium value on the average of 10^5/ml. Our model gives a simi-

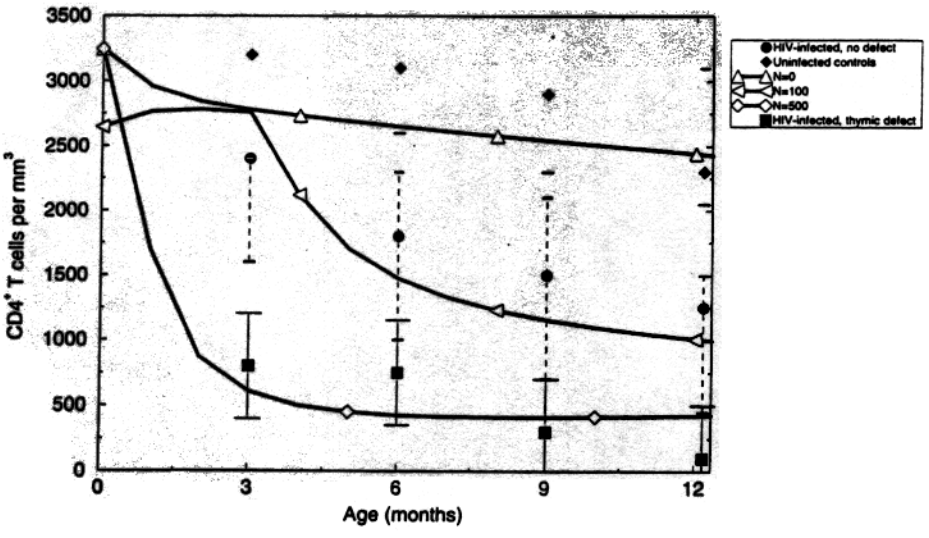

FIG. 6. This figure compares three different model runs with data from the study of Kourtis et al. (14). The three groups presented from the study represent (◇) an uninfected cohort, (■) an HIV-infected cohort with thymic defects, and a (●) an HIV-infected cohort with no thymic defect. These infection groups are presented with three model runs using three different viral productions based on the formula

$$N(t) = N_0\left(1 + \frac{2.5t^2}{1.6 \times 10^6 + t^2}\right),$$

with $N_0 = 0$, 100, 500.

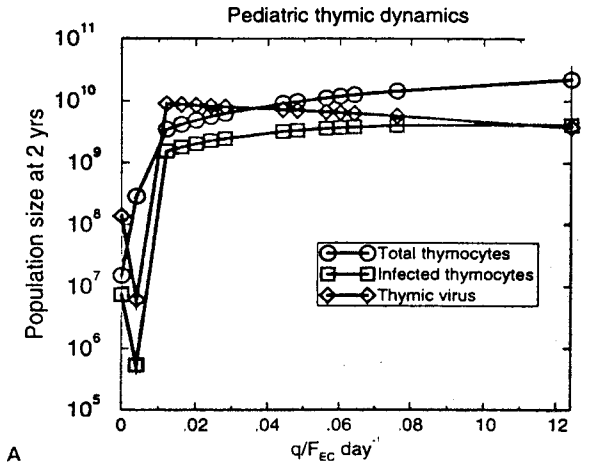

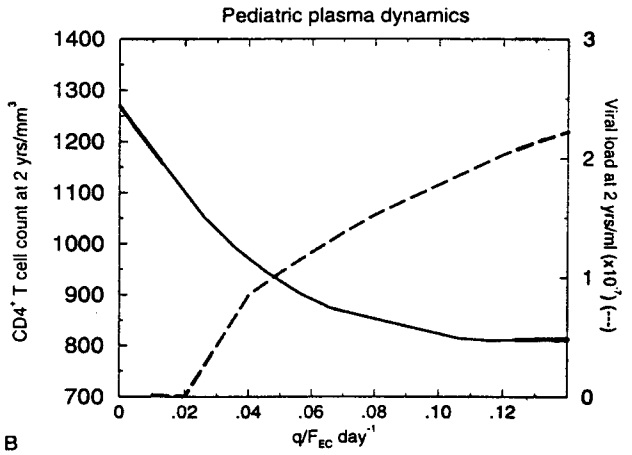

FIG. 7. The role of viral transport into and out of the thymus is studied. All parameters are fixed, and only the quantity q/F_{EC} is varied. The steady state levels for each of the populations are given. Shown are the dynamics for the combined thymic-plasma model of pediatric HIV-1 infection. (**A**) The thymic compartment dynamics. (**B**) The plasma compartment dynamics. The pediatric runs are over a 2-year period since birth.

lar dynamic, with viral loads leveling to 10^7/ml. The reason for the difference in quasi–steady state viral loads is unknown. One possibility is that the rate of viral exchange between the thymus and the body is lower than we have assumed. Thus, if we lower the value of q/F_{EC} (Fig. 7) we can obtain similar quasi–steady state viral levels. Another possibility is that one or more parameters that describe viral dynamics or the immune response to the virus are different in children than in adults. Data from clinical trials of combination therapy in pediatric patients should soon be available and should yield estimates of the relevant dynamic parameters in children.

We again explore the role of the infection rate, β_p, in the infection dynamics. We fix all parameters and vary only the rate constant, β_p. Figure 8 shows how the number of CD4$^+$ T cells in an HIV infant up to 2 years after birth varies with β_p. The higher β_p, the stronger the infection is, and also the faster the decrease to lower T-cell numbers. The dependence on the value of β is similar, though weaker.

Reports have been published of HIV-1–positive infants that appear to have cleared HIV and eventually have become HIV-1–negative (54,55). Although laboratory errors cannot be completely ruled out, these results raise the possibility that in some children infection is transient. The phenomenon of transient infection occurs in our model if $N\beta$ is lower than a critical value, where N is the viral burst size and β the rate of infection per T cell. If either N or β are typically lower in infants than in adults, then transient infection could be more common in

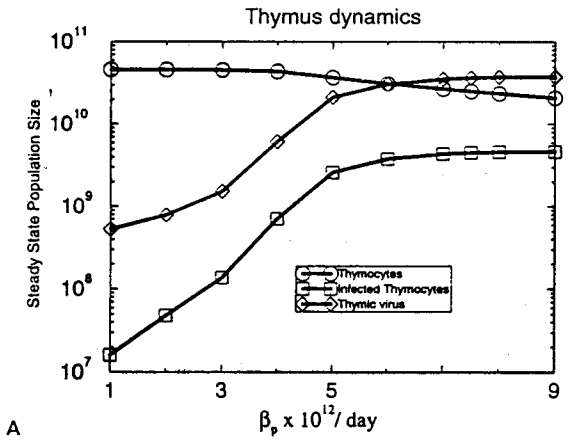

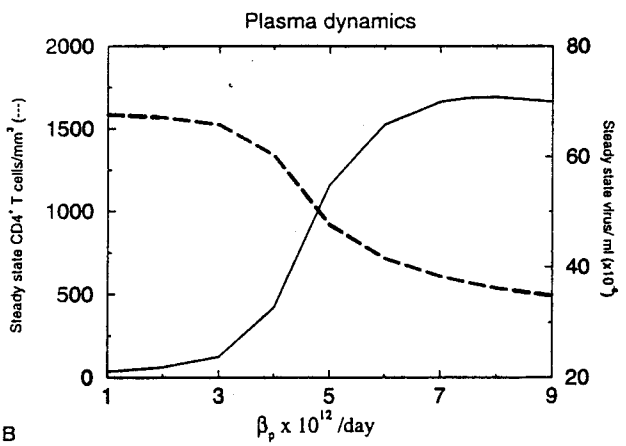

FIG. 8. The pediatric-combined model's dependence on the infection rate β_p is explored. The steady state values of (**A**) total thymocytes, infected thymocytes and thymic virus, and (**B**) T cells and plasma virus are shown as β_p varies.

infants than in adults. Lower viral production (N) might occur because the viral strain present is a slow/low strain; and lower values of β might occur if immune activation is lower in these infants than adults.

DISCUSSION

The aim of this study was to examine the role that HIV-1 infection of the thymus plays in the overall dynamics of pediatric HIV infection. We used mathematical modeling of the dynamics of uninfected and infected thymocytes, and of the virus in the thymus, to study HIV-1 infection of the precursors to $CD4^+$ T cells. Inasmuch as almost all thymocytes express some level of the CD4 cell surface molecule, which may render them susceptible to HIV-1 infection, all thymocyte subsets were treated as one population. The parameters governing uninfected thymocyte death, differentiation into mature T cells, and population growth are average values based on previous experimental and theoretical studies and resulted in realistic dynamics of the thymocyte population. Conversely, the parameters governing the infection of thymocytes, and the dynamics of the virus and infected thymocytes are not yet fully known. Data are available from two experimental systems, in vitro infection of thymocytes, and infection of human fetal thymus implants in SCID mice. However, the rate of infection and viral production in these systems probably give an overestimate of the rate of disease progression in the intact human thymus in vivo, in which the immune response to HIV-1 may, to some extent, keep the infection in check. Rates of viral production estimated for mature T cells are also likely to give an overestimate of viral production by thymocytes. Because of their short life span and higher sensitivity to the induction of apoptosis, each infected thymocyte is likely to produce fewer viral particles before it dies than an infected T cell. Nevertheless, we used these parameters as a starting point for our exploration of the model and studied the sensitivity of the results to variations of these parameters.

Several important points emerge from our study. First, to achieve a reduction of about twofold in thymocyte numbers, as observed in autopsies of patients (42), it is sufficient to assume a viral production which is equal or less than that estimated for peripheral T cells in lymphoid tissue (N_T on the order of 100), and a low rate constant for thymic infection (β_p on the order of 10^{-10} day^{-1}). It is not unreasonable to accept that a low intrathymic infection rate could suffice to maintain infection, because the thymus is a dense tissue in which thymocytes are closely packed together. Indeed, in our model, $\beta_p T_p$ is of order 1 infection event per virion per day, which is actually higher than the corresponding quantity for peripheral T cells, βT, which is on the order of 10^{-3} infection events per virion per day. This difference is explored in section on Pediatric Parameters for the Thymus-Plasma Model.

Second, the results are highly sensitive to the value of either N_T or β_p—realistic dynamics are obtained only in a narrow regime of the parameter space. The combination of these two parameters determines the fate and rapidity of the infection in the model. The product $N_T\beta_p$ can be viewed as a measure of HIV's virulence. If $N_T\beta_p$ is less than a critical value, then thymic infection is not established. A similar result was previously obtained for peripheral infection in models (47,48,56). Thus, the model suggests that a critical level of virulence is needed for HIV-1 to establish an infection in the thymus successfully, as well as a similar critical level in the periphery.

Third, the results are also sensitive to the rates of viral clearance and export. Obviously, the faster the rate the virus is cleared from the thymus, the slower the infection is, and a fast rate of clearance could even account for a decay of the infection.

Using a combined model of the dynamics of virus, $CD4^+$ peripheral T-cell and thymocyte populations, we show that the decline in $CD4^+$ peripheral T-cell levels, in spite of the low fraction of productively infected cells in the peripheral blood, is more readily modeled when we take into account the depletion, as a result of infection of $CD4^+$ T-cell precursors in the thymus, as compared with previous results in Perelson et al. (48). Thus, the thymic production of T cells is important in pediatric patients, in which HIV infection of the thymus has a more severe effect than in adult patients.

Rates of disease progression in infants are variable. Some infants progress to AIDS rapidly after birth, others somewhat more slowly; but in either case, children tend to progress to AIDS much more rapidly than adults (14–17). In most cases, the thymus of pediatric HIV-positive patients does not have the chance to develop normally (as seen in autopsies) (33) and therefore may contribute to the more rapid $CD4^+$ T-cell depletion typical of pediatric AIDS cases. This suggests that understanding the events that alter the normal development of the thymus may lead to a better understanding of pediatric infection with HIV.

The rate of recovery of $CD4^+$ T cells after chemotherapy and irradiation (administered to cancer patients) is inversely correlated to patient's age: in children, $CD4^+$ T-cell levels may recover to pretreatment levels in a few months, whereas in adults these levels rarely recover to pretreatment levels even 18 months after treatment (57).

Examination of the ratio of naive (CD45RA+) to experienced (CD45RO+) peripheral CD4+ T cells in the recovering patients suggests that the activity of the thymus, even residual activity sometimes seen in adult patients, is crucial for CD4+ T-cell recovery from severe depletion (57). Thymic involution seems to affect the helper T-cell compartment most (58). The thymic production of CD4+ T cells decreases with age, suggesting that the importance of the thymus in HIV-1 infection may also decrease as the individual ages. Even so, differences in thymic production may explain part of the variability in disease progression in adults as well as children.

In this context, recent findings (59–62) suggest that mature, functional CD4+ T cells within the thymus exert several feedback effects on the developing thymocytes. These effects include limiting the overall production of thymocytes and controlling the CD4:CD8 ratio of the T cells that are produced. Analyzing experiments on CD4+ T-cell depletion in mice showed that these feedback effects would further decrease thymic production of CD4+ T cells (63). If similar feedback regulation occurs in the human thymus, the destruction of this regulation may further increase the CD4+ T-cell depletion during HIV-1 infection.

Finally, the role of the secondary lymph system is being increasingly recognized as the major site of HIV infection dynamics. A model of viral dynamics and transport between the blood and the lymphoid system could better elucidate these overall dynamics. In particular, the role of the follicular dendritic cells in collecting virions may play a key role in the viral dynamics in that compartment. Moreover, an assumption inherent in our model is that thymocytes are constantly activated. In secondary lymphoid tissue and plasma, only a small fraction of lymphocytes are activated. Thus, the model presented here cannot be applied without modification to multicompartment models of HIV infection that incorporate lymph nodes and spleen. This difference may be a key feature of any lymph system model of HIV progression. A recent model by Stekel et al. (64) explores these features.

To summarize, we have developed a mathematical model of HIV infection of the thymus. The model suggests that thymic infection can occur rapidly, and that the thymus can serve as a reservoir for virus. Our numerical studies point out the importance of gaining further information about the parameters that govern the dynamics of HIV infection, and, in particular, the transport of viral particles between compartments. The role of the thymus in infection may be the explanation for the early and high viral loads seen in pediatric patients.

APPENDIX

Analysis of the Thymus Model

In the absence of virus infection, we assume that the thymocyte population is at its the steady state value:

$$T_p^0 = \frac{T_p^{max}}{2r_p}\left(g + \sqrt{g^2 + \frac{4sr_p}{T_p^{max}}}\right), \qquad [14]$$

where $g \equiv r_p - \delta_{T_p} - e_1$. For the parameter values in Table 1, $g = 0.76$ day^{-1} and $T_p^0 = 2.5 \times 10^{10}$. We use this *uninfected* steady state as the initial condition for simulations of HIV infection.

We introduce infection by having peripheral virus enter the thymus at a constant rate s_V. Exploring the steady states of Equations 1 through 3, we find two things. First, with $s_V > 0$, there is no *uninfected steady state.*

The steady states of the system are found by solving

$$0 \doteq s - \delta_{T_p} T_p - e_1 T_p + r_p T_p\left(1 - \frac{T_p + T_p^*}{T_p^{max}}\right) - \beta_p V_T T_p, \qquad [15]$$

$$0 = \beta_p V_T T_p - \delta_{T_p^*} T_p^* - e_2 T_p^*, \qquad [16]$$

$$0 = s_V + N_T \delta_{T_p^*} T_p^* - c_V V_T - \beta_p V_T T_p. \qquad [17]$$

If we substitute

$$h = \frac{1}{\delta_{T_p^*} + e_2} \qquad [17a]$$

equations (16) and (17) give

$$\bar{T}_p^* = h\beta_p \bar{T}_p \bar{V}_T \qquad [18]$$

and

$$\bar{V}_T = \frac{s_V}{c_V + \bar{\beta}_p \bar{T}_p (1 - hN_T \delta_{T_p^*})} \qquad [19]$$

For $\bar{V}_T$ to be positive, it is sufficient that

$$\beta_p N_T < \frac{(c_V + \beta_p \bar{T}_p)}{h\bar{T}_p \delta_{T_p^*}} \equiv (\beta_p N_T)_{crit} \qquad [20]$$

The value of $(\beta_p N_T)crit$ varies depending on parameter values. This is topic is explored further in the body of the article. Note that the parameters c_V, $\delta_{T_p^*}$, and e_2 are all critical and that each can result in a similar dynamic scheme.

Because the steady state values $\bar{V}_T$ and $\bar{T}_p^*$ depend on the steady state value $\bar{T}_p$, it suffices to find the value for $\bar{T}_p$ and then calculate the other values. To this end, it is necessary to determine the roots of a cubic expression in

$\bar{T}_p$ (from Equation 15 with Equations 16 and 17, $c_1 T_p^3 + c_2 T_p^2 + c_3 T_p + c_4 = 0$, where the coefficients $c_1 \ldots c_4$ are complicated functions of the parameters. Multiple roots for this equation may exist. For the parameter values discussed in the section Parameter Estimates, there are two positive roots (steady states) and one negative root. The values of N_T and β_p determine which of the positive roots is the stable steady state.

Acknowledgments: This work was supported under grant number DMS 9596073 from the National Science Foundation. Portions of this work were also performed under the auspices of the U.S. Department of Energy and supported by NIH grants RR06555 and AI28433. This work is also supported by the Santa Fe Institute and the Joseph P. Sullivan and Jeanne M. Sullivan Foundation. The simulations were carried out using *Mathematica* (65).

REFERENCES

1. Fauci AS. The human immunodeficiency virus: infectivity and mechanisms of pathogenesis. *Science* 1988;239:617–22.
2. Cantor H, Weismann IL. Development and function of subpopulation of thymocytes and T lymphocytes. *Prog Allergy* 1976; 20:1–64.
3. Spangrude GJ, Scollay R. Differentiation of hematopoietic stem cells in irradiated mouse thymic lobes. Kinetics and phenotype of progeny. *J Immunol* 1990;145:3661–8.
4. Janeway CA. Thymic selection: two pathways to life and two to death. *Immunity* 1994;1:3–6.
5. Bonyhadi ML, Rabin L, Salimi S, et al. HIV induces thymus depletion in vivo. *Nature* 1993;363:728–32.
6. Su L, Kaneshima H, Bunyhadi M, et al. HIV-1-induced thymocyte depletion is associated with indirect cytopathicity and infection of progenitor cells in vivo. *Immunity* 1996;2:25–36.
7. Schnittman SM, Singer KH, Greenhouse JJ, et al. Thymic microenvironment induces HIV expression. Physiologic secretion of IL-6 by thymic epithelial cells up-regulates virus expression in chronically infected cells. *J Immunol* 1991;147:2553–8.
8. Stanley SK, McCune JM, Kaneshima H, et al. Human immunodeficiency virus infection of the human thymus and disruption of the thymic microenvironment in the SCID-hu mouse. *J Exp Med* 1993;178:1151–63.
9. Prevot S, Audouin J, Andre-Bougaran J, et al. Thymic pseudotumorous enlargement due to follicular hyperplasia in a human immunodeficiency virus sero-positive patient. Immunohistochemical and molecular biological study of viral infected cells. *Am J Clin Pathol* 1992;97:420–5.
10. Hays EF, Uittenbogaart CH, Brewer JC, et al. In vitro studies of HIV-1 expression in thymocytes from infants and children. *AIDS* 1992;6:265–72.
11. Mano H, Chermann JC. Fetal human immunodeficiency virus type 1 infection of different organs in the second trimester. *AIDS Res Hum Retroviruses* 1991;7:83–8.
12. Meyers A, Pepe N, Cranley W, McCarten K. Decreased thymus size on chest radiography: a sign of pediatric human immunodeficiency virus infection? *Pediatrics* 1992;90:99–102.
13. Tanaka KE, Hatch WC, Kress Y, et al. HIV-1 infection of human fetal thymocytes. *J AIDS* 1992;5:94–101.
14. Kourtis AP, Ibegbu C, Nahmias AJ, et al. Early progression of disease in HIV-infected infants with thymus dysfunction. *N Engl J Med* 1996;335:1431–6.
15. Levy JA. Pathogenesis of HIV infection. *Microbiol Rev*1993;57: 183–289.
16. Oxroby MJ. Vertically acquired HIV infection in the US. In Pizzo PA, Wilfert CM, eds. *Pediatric AIDS: the challenge of HIV infection in infants, children and adolescents*, 2nd ed. Baltimore: Williams & Wilkins, 1994:20–30.
17. Frederick T, Mascola L, Eller A, O'Neil L, Byers B. Progression of HIV disease among infants and children infected perinatally with HIV or through neonatal blood transfusion. *Pediatr Infect Dis J* 1994;13:1091–7.
18. Palumbo PE, Kwok S, Waters S, et al. Viral measurements by PCR-based assays in HIV-infected infants. *J Pediatr* 1995;126: 592–5.
19. Mcintosh K, Shevitz A, Zaknun D, et al. Age- and time-related changes in extracellular viral load in children vertically infected by HIV. *Pediatr Infect Dis J* 1996;15:1087–91.
20. Marshall C, Conway B, Allen UD, et al. Evaluation of virologic parameters as potential predictors of advanced disease in HIV-infected Canadian children, Int Conf AIDS July 7–12 11:233 (abstract no. Tu.B.193).
21. Dolfus C, Courpotin C, Jacomet C, et al. Pediatric HIV-1 infection and viral quantification [abstract Tu.B.2370. XI International Conference on AIDS, 1996;11:329.
22. Schnittman SM, Denning SM, Greenhouse JJ, et al. Evidence for susceptibility of intrathymic T-cell precursors and their progeny carrying T-cell antigen receptor phenotypes TCR alpha beta + and TCR gamma delta + to human immunodeficiency virus infection: a mechanism for CD4+ (CD4+ T) lymphocyte depletion. *Proc Natl Acad USA* 1990;87:7727–31.
23. De Rossi A, Calabro ML, Panozzo M, et al. In vitro studies of HIV-1 infection in thymic lymphocytes: a putative role of the thymus in AIDS pathogenesis. *AIDS* 1990:6:287–98.
24. Mehr R, Globerson A, Perelson A. Modeling positive and negative selection and differentiation processes in the thymus. *J Theor Biol* 1995;175:103–126.
25. Mehr R, Globerson A, Perelson A. Models for selection processes in the thymus. *J Appl Sci Comput* 1996;3:1–19.
26. Mehr R, Abel L, Ubezio P, Globerson A, Agur Z. A mathematical model of the effect of aging on bone marrow cells colonizing the thymus. *Mech Ageing Dev* 1993;67:159–72.
27. Shortman K, Egerton M, Spangrude GJ, Scollay R. The generation and fate of thymocytes, *J Semin Immunol* 1990;2:3–12.
28. Ho DD, Neumann AU, Perelson AS, et al. Rapid turnover of plasma virions and CD4+lymphocytes in HIV-1 infection. *Nature* 1995;373:123–6.
29. Westermann J, Pabst R. Distribution of lymphocyte subsets and natural killer cells in the human body. *Clin Invest* 1992;70:539–44.
30. Haase AT, Henry K, Zupancic M, et al. Quantitative image analysis of HIV-1 infection in lymphoid tissue. *Science* 1996;274: 985–9.
31. Perelson AS, Neumann AU, Markowitz M, Leonard JM, Ho DD. HIV-1 dynamics in vivo: virion clearance rate, infected cell life span, and viral generation time. *Science* 1996;271:1582–6.
32. Autran B, Guiet P, Raphael M, et al. Thymocyte and thymic microenvironment alterations during a systemic HIV infection in a severe combined immunodeficient mouse model. *AIDS* 1996;10: 717–27.
33. Grody WW, Fligiel S, F. Naeim. Thymus involution in the acquired immunodeficiency syndrome. *Am J Clin Pathol* 1985;84: 85–95.
34. Lafeuillade A, Poggi C, Profizi N, et al. Human immunodeficiency virus Type 1 in lymph nodes compared with plasma. *J Infect Dis* 1996;174:404–7.
35. Kirschner D, Webb GF. A mathematical model of combined drug therapy of HIV infection. *J Theor Med* 1997;1:25–34.
36. Kirschner D, Webb GF. Resistance, remission, and qualitative differences in HIV chemotherapy. *Emerg Infect Dis* 1997;3:273–83.
37. Hueber AO, Raposo G, He HT. Thy-1 triggers mouse thymocyte apoptosis through a bcl-2-resistant mechanism. *J Exp Med* 1994; 179:785–96.
38. Kubo S, Nakayama T, Furutani-Seiki M, et al. A novel form of self

tolerance dictated in the thymus of transgenic mice with autoreactive TCR alpha and beta chain genes. *Int Immunol* 1994;6:593–602.
39. Bofill M, Janossy G, Lee CA, et al. Laboratory control values for CD4 and CD8 T lymphocytes. *Clin Exp Immunol* 1992;88:243–52.
40. Shearer WT, Quinn TC, LasRussa P, et al. Viral load and disease progression in infants infected with HIV-1, *N Engl J Med* 1997; 336:1337–42.
41. Kendall M. *The Thymus Gland.* London: Academic Press, 1981.
42. Cardarelli N. *The Thymus in Health and Senescence*, Vol. 1. Boca Raton, FL: CRC Press, 1989.
43. Salinas F, Smith L, Goodman J. Cell size distribution in the thymus as a function of age. *J Cell Physiol* 1972;80:339–45.
44. Tosi P, Kraft R, Luzi P, et al. Involution patterns of the human thymus: size of the cortical area as a function of age. *Clin Exp Immunol* 1982;47:497–504.
45. Guthrie HA. *Introductory Nutrition*, 6th ed. St. Louis: Times College Publishing, 1986.
46. McInney RE, Wilfert CM. Lymphocyte subsets in children younger than 2 years old: normal values in population at risk for HIV infection and diagnostic and prognostic application to infected children. *Pediatr Infect Dis J* 1992;11:639–44.
47. Perelson AS. Modeling the interaction of the immune system with HIV. In Castillo-Chavez C, ed. *Mathematical and statistical approaches to AIDS epidemiology. Lecture notes in biomathmatics, vol. 83.* New York: Springer-Verlag, 1989:350–70.
48. Perelson AS, Kirschner D, DeBoer RJ. The dynamics of HIV infection of CD4$^+$ T cells. *Math Biosci* 1993;114:81–125.
49. Wei X, Ghosh SK, Taylor ME, et al. Viral dynamics in human immunodeficiency virus type 1 infection. *Nature* 1995;373:117–22.
50. McLean AR, Emery VC, Webster A, Griffiths PD. Population dynamics of HIV within an individual after treatment with zidovudine. *AIDS* 1991;5:485–9.
51. Phillips AN. Reduction of HIV concentration during acute infection: independence from a specific immune response. *Science* 1996;271:497–9.
52. Hammer JA. Die Menschen Thymus, in Gesuundt and Krankheit, Part 1. *Mikrosk Anat Forsch* 1926:6(suppl.):107–208.
53. Schnittman SM, Greenhouse JJ, Psallidopoulos MC, et al. Increasing viral burden in CD4$^+$ T cells from patients with human immunodeficiency virus (HIV) infection reflects rapidly progressive immunosuppression and clinical disease. *Ann Intern Med* 1990;113: 438–43.
54. Bryson YJ, Pang S, Wei LS, Dickover R, Diagne A, Chen IS. Clearance of HIV infection in a perinatally infected infant. *N Engl J Med* 1995;332:833–8.
55. Newell ML, Dunn D, De Maria A, et al. Detection of virus in vertically exposed HIV-antibody-negative children. *Lancet* 1966; 347:213–5.
56. Perelson AS. Two theoretical problems in immunology: AIDS and epitopes. In Cowan G, Pines D, Meltzer D, eds. *Complexity: metaphors, models and reality.* Reading, MA: Addison-Wesley, 1994: 185–97
57. Mackall CL, Fleischer TA, Brown MR, et al. Age, thymopoiesis, and CD4$^+$ T-lymphocyte regeneration after intensive chemotherapy. *N Engl J Med* 1995;332:143–9.
58. Green-Johnson J, Wade AW, Szewczuk MS. The immunobiology of aging. In Cooper EL, Nisbet-Brown E, eds. *Developmental immunology.* New York: Oxford University Press, 1993:427–51.
59. Fridkis-Hareli M, Mehr R, Abel L, Globerson A. Developmental interactions of CD4$^+$ T cells and thymocytes: age-related differential effects. *Mech Ageing Dev* 1994;73:169–78.
60. Mehr R, Perelson A, Globerson A. Feedback regulation of T cell development in the thymus. *J Theor Biol* 1996;181:157–67.
61. Mehr R, Perelson AS, Fridkis-Hareli M, Globerson A. Feedback regulation of T cell development: manifestations in aging. *Mech Ageing Dev* 1996;19:195–210.
62. Mehr R, Perelson AS, Fridkis-Hareli M, Globerson A. Regulatory feedback pathways in the thymus. *Immunol Today* 1997;18:581–5.
63. Mehr R, Perelson AS. Blind homeostasis and the CD4/CD8 ratio in the thymus and peripheral blood. *J Acquir Immune Defic Syndr Hum Retrovirol* 1997;14:387–98.
64. Stekel DJ, Parker CE, Nowak MA. A model of lymphocyte recirculation. *Immunol Today*1997;18:216–21.
65. Wolfram SA. *Mathematica: a system for doing mathematics by computer.* Reading, MA: Addison-Wesley, 1988.